Functions of Chloroplastic Adenylate Kinases in Arabidopsis[1][W][OA]

Peter Robert Lange[2], Claudia Geserick, Gilbert Tischendorf, and Rita Zrenner*

Max-Planck-Institut für Molekulare Pflanzenphysiologie, 14476 Golm, Germany (P.R.L., C.G., R.Z.); and Freie Universität Berlin, Institut für Biologie, Pflanzenphysiologie, 14195 Berlin, Germany (G.T.)

Adenosine monophosphate kinase (AMK; adenylate kinase) catalyses the reversible formation of ADP by the transfer of one phosphate group from ATP to AMP, thus equilibrating adenylates. The Arabidopsis (*Arabidopsis thaliana*) genome contains 10 genes with an adenylate/cytidylate kinase signature; seven of these are identified as putative adenylate kinases. Encoded proteins of at least two members of this Arabidopsis adenylate kinase gene family are targeted to plastids. However, when the individual genes are disrupted, the phenotypes of both mutants are strikingly different. Although absence of AMK2 causes only 30% reduction of total adenylate kinase activity in leaves, there is loss of chloroplast integrity leading to small, pale-looking plantlets from embryo to seedling development. In contrast, no phenotype for disruption of the second plastid adenylate kinase was found. From this analysis, we conclude that AMK2 is the major activity for equilibration of adenylates and de novo synthesis of ADP in the plastid stroma.

Nucleotides are essential metabolites in a multitude of biochemical and developmental processes. Nucleotide levels depend on the interaction of purine and pyrimidine de novo synthesis and the respective degradation pathways, salvage reactions that recycle nucleosides and free bases, and phosphotransfer reactions that convert mono- and dinucleotides to the triphosphate form (Zrenner et al., 2006). Nucleoside monophosphate (NMP) kinases catalyze the reversible transfer of one phosphate group of a donor nucleotide (ATP) to an acceptor NMP to generate ADP and a nucleoside diphosphate. Whereas the specificity for the phosphate donor is not very strict, the accepting NMP is recognized with specificity (Rudolph et al., 1999). In many organisms ranging from bacteria to animals, adenylate kinase has been shown to phosphorylate the nucleotide AMP to form ADP (Buchanan and Hartmann, 1959; Neuhard and Nygaard, 1987; Christopherson and Szabados, 1997). Thus, adenylate kinase is required for interconversion of adenine nucleotides (ATP + AMP ↔ 2 ADP) and is considered to be a key enzyme activity in energy metabolism, equilibrating adenine nucleotides in vivo (Pradet and Raymond, 1983; Igamberdiev and Kleczkowski, 2006). Therefore, adenylate kinase plays a fundamental role for the adenylate energy charge that is highly important in all organisms for metabolic processes and growth (Atkinson, 1968; Chapman et al., 1971).

Biochemical studies have shown the presence of this enzyme reaction in plants (Bomsel and Pradet, 1968). The bulk activity of adenylate kinase is located in the chloroplast stroma and in the intermembrane space of the mitochondria (Birkenhead et al., 1982; Hampp et al., 1982; Stitt et al., 1982). However, there are few studies analyzing the distribution of nucleotide pools in relation to metabolism or plant development (Wagner and Backer, 1992; Geigenberger and Stitt, 2000; Igamberdiev and Kleczkowski, 2006). On a cellular level, approximately 45% of the adenine nucleotides are located in the plastid stroma, 46% in the cytosol, and 9% in mitochondria of leaves (Stitt et al., 1982, 1989; Farre et al., 2001). The reaction catalyzed by adenylate kinase is close to equilibrium in the plastid stroma and in the cytosol, but not in mitochondria (Stitt et al., 1982) due to lack of adenylate kinase activity in the mitochondrial matrix.

Database screening revealed that the genome of Arabidopsis (*Arabidopsis thaliana*) contains 10 genes with an adenylate/cytidylate kinase signature. To date, two of these genes have been further characterized; *At5g26667* was identified as UMP/CMP kinase (Zhou et al., 1998), and *At2g37350* was described as a plastidic adenylate kinase (Carrari et al., 2005). Analysis of T-DNA insertion mutants disrupted in *At2g37350* revealed increased amino acid levels and enhanced root growth without a strong phenotypic impact (Carrari et al., 2005). Here, we present the functional analysis of two further adenylate kinases (*At5g47840* and *At5g35170*). Both nuclear genes encode isoforms that include a plastid targeting sequence.

[1] This work was supported by the Deutsche Forschungsgemeinschaft (fellowship no. Zr3/2 to R.Z.) as part of The *Arabidopsis* Functional Genomics Network, and by the Max-Planck-Society.

[2] Present address: Leibniz-Institut für Pflanzenbiochemie, Weinberg 3, 06120 Halle, Germany.

* Corresponding author; e-mail zrenner@mpimp-golm.mpg.de.

The author responsible for distribution of materials integral to the findings presented in this article in accordance with the policy described in the Instructions for Authors (www.plantphysiol.org) is: Rita Zrenner (zrenner@mpimp-golm.mpg.de).

[W] The online version of this article contains Web-only data.

[OA] Open Access articles can be viewed online without a subscription.

www.plantphysiol.org/cgi/doi/10.1104/pp.107.114702

However, the individual phenotypes of these two *amk* (adenosine monophosphate kinase) mutants are strikingly different. Disruption of *At5g47840* leads to loss of chloroplast integrity, causing a bleached phenotype from early embryo to seedling development. In contrast, no phenotype for the disruption of *At5g35170* was found.

RESULTS

Phylogenetic Analysis of Adenylate Kinase Isoforms

For phylogenetic analysis, we used all 10 Arabidopsis kinases that belong to the same class of aspartokinases (Cheek et al., 2002), including one that has already been functionally characterized (Carrari et al., 2005) and the one that has been described as uridylate kinase (Zhou et al., 1998). We integrated the potato (*Solanum tuberosum*) adenylate kinase (Regierer et al., 2002) and all members of the same class of rice (*Oryza sativa*). A phylogenetic tree was constructed containing the complete sequences of the predicted proteins (Fig. 1A). Several software tools for prediction of intracellular localization were used. Plants stably expressing GFP-fusions with AMK1, AMK2, AMK3, AMK5, and AMK7 were investigated for the subcellular localization of proteins in this family. The phylogenetic tree shows that putative AMKs form distinct branches, whereas all uridylate kinases are on a separate branch (Fig. 1A, blue branch; uridylate kinase activity data not shown).

The first branch of adenylate kinases contains two isoforms of Arabidopsis and two of rice. All these proteins are presumably cytosolic (Fig. 1A, yellow branch), as they are predicted not to have any signal, mitochondrial targeting, or chloroplast transit peptide. This was confirmed by stably transformed GFP-fusion with AMK3 (Fig. 1B, 1 and 2), but in subcellular proteome analyses both proteins (AMK3 and AMK4) were found in mitochondria (Millar et al., 2001; Heazlewood et al., 2004). It has been shown for other cytosolic proteins that association to mitochondria is possible (Giege et al., 2003), but AMK3 and AMK4 without GFP-fusion indeed may localize between the outer and inner membrane of mitochondria to form the previously reported mitochondrial adenylate kinase activity (Birkenhead et al., 1982; Hampp et al., 1982; Stitt et al., 1982).

AMK2 and AMK5 together with two rice homologs are phylogenetically distinct and form the predicted plastid branch of plant adenylate kinases (Fig. 1A, green branch). The targeting of stably transformed GFP-fusions confirmed their plastidic localization (Fig. 1B, 3–6). This was supported by subcellular proteome analysis, where a stromal localization of AMK2 (Peltier et al., 2006) and a thylakoid- and envelope-associated localization of AMK5 were found (Froehlich et al., 2003; Peltier et al., 2004).

The more distantly related sequences are the previously characterized Arabidopsis AMK1, the potato ADK, and two further Arabidopsis AMKs together with three homologs of rice (Fig. 1A, gray branch). In comparison with adenylate kinases of other organisms (data not shown), this branch contains exclusively plant sequences. The closest homologs are from endoparasites like *Plasmodium falciparum* or *Babesia bovis*. Our study using a stably transformed GFP-fusion with AMK1 and transient expression of a GFP-fusion with AMK7 revealed mitochondrial localization of both proteins (Fig. 1B, 7–11). In contrast to these findings, there is a previous report describing particle bombardment with an AMK1 GFP-fusion construct and reduced adenylate kinase activity in isolated chloroplasts of mutants with disruption of *AMK1*. This led to the conclusion that AMK1 is located in plastids (Carrari et al., 2005). These conflicting results of AMK1 localization might be caused by dual targeting, as it has been found for aminoacyl-tRNA synthetases (Duchene et al., 2005; Millar et al., 2006). Further analysis of this detail is not within the scope of this study. Because expression analysis using quantitative real-time reverse transcription (RT)-PCR revealed low transcript levels for *AMK6* and *AMK7*, it is not surprising that these proteins together with AMK1 were not monitored in subcellular proteome studies. Several tools for predicting the subcellular localization resulted in highly probable mitochondrial targeting of most members of this clade.

Correlation Analysis of Adenylate Kinase Expression in Arabidopsis

To elucidate putative specific functions, we screened available expression data for transcriptional co-regulation with all *AMK*s. Unfortunately, not all genes are represented on the Affymetrix ATH1 microarray including *AMK6*. Therefore, we also analyzed the expression patterns using quantitative real-time RT-PCR (Fig. 2A), confirming that *AMK1* to *AMK5* are much higher expressed than *AMK6*, while *AMK7* is at the detection limit. Using the Arabidopsis co-response database (Steinhauser et al., 2004), we searched for transcriptional correlations using transcript profiles of all Arabidopsis tissues of the AtGenExpress developmental series (Schmid et al., 2005) and the nonparametric Spearman's Rho rank correlation with Bonferroni correction. To visualize significant correlations with genes involved in metabolic pathways, we used the MapMan ontology, assigning genes to more than 800 hierarchical categories (Thimm et al., 2004; Usadel et al., 2005). Together with the visualization tool PageMan (Usadel et al., 2006) and the statistical analysis using Wilcoxon's test, including the correction of multiple testing by Bonferroni, we identified those categories whose members show a coordinated response together with the respective *AMK*, which is statistically significant compared with all other genes. *P* values were assigned a positive or negative value, depending on whether the correlation was positive or negative, and visualized on a false color scale, with increasing blue

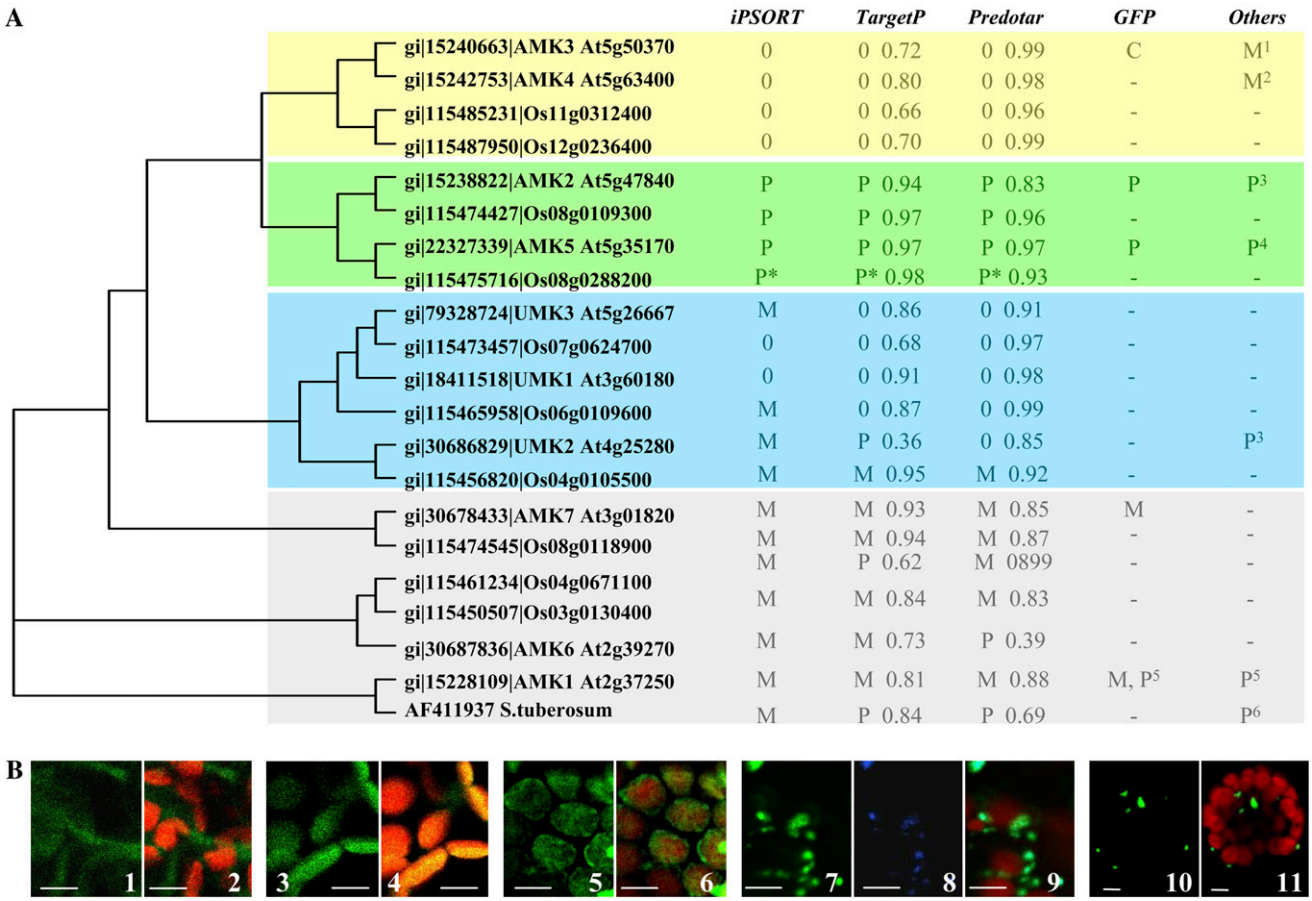

Figure 1. Comparison of NMP kinases. A, Comparison of all Arabidopsis and rice NMP kinase proteins containing Inter-Pro signature IPR011769. Predictions of intracellular localization of mature proteins were performed with iPSORT, TargetP, and Predotar. Method intern scores for the predictions are shown, and the results are classified as follows: 0, predicted as having no signal, mitochondrial targeting, or chloroplast transit peptide; M, predicted as having a mitochondrial targeting peptide; P, predicted as having a chloroplast targeting peptide. Our GFP results and the summary of other studies are classified as follows: C, protein found in the cytosol; M, protein associated to mitochondria; P, protein associated to plastids. 1, Millar et al. (2001); 2, Heazlewood et al. (2004); 3, Peltier et al. (2006); 4, Peltier et al. (2004); 5, Carrari et al. (2005); 6, Regierer et al. (2002); *, annotated Os08g0288200 is presumably not full length; therefore, an assembly of CT842017 and AK070372 was translated and used for analysis. B, Fluorescence signals of leaf mesophyll cells. 1, AMK3-GFP, GFP fluorescence signal (green); 2, AMK3-GFP, overlay of GFP and chlorophyll autofluorescence signal (red); 3, AMK2-GFP, GFP fluorescence signal; 4, AMK2-GFP, overlay of GFP and chlorophyll autofluorescence signal; 5, AMK5-GFP, GFP fluorescence signal; 6, AMK5-GFP, overlay of GFP and chlorophyll autofluorescence signal; 7, AMK1-GFP, GFP fluorescence signal; 8, AMK1-GFP, DsRed fluorescence signal of the transiently transformed mitochondrial marker DHODH-DsRed (blue); 9, AMK1-GFP, overlay of GFP, DsRed, and chlorophyll autofluorescence signal; 10, AMK7-GFP, GFP fluorescence signal of transiently transformed protoplasts; 11, AMK7-GFP, overlay of GFP and chlorophyll autofluorescence signal; white bars = 4 μm.

and red indicating an increasingly and decreasingly significant correlation, respectively. All significant MapMan categories of metabolic processes that match our high stringent selection criteria are visualized in Figure 2B.

The co-response analysis showed distinct expression patterns for *AMK*s that are located on the previously identified phylogenetic branches. While *AMK2* and *AMK5* expression was positively correlated with the expression of genes involved in photosynthesis and major carbohydrate metabolism, the expression of *AMK3*, *AMK4*, and *AMK1* was negatively correlated with genes of photosynthesis and uncorrelated with genes of carbohydrate metabolism. Whereas no significant correlation was detectable between the expression of *AMK2*, *AMK5*, *AMK3*, and *AMK4* with genes of glycolysis, tricarboxylic acid cycle, mitochondrial electron transport, and ATP synthesis, a significant positive correlation was found for the expression of *AMK1* with genes of light-independent energy metabolism. All these correlations were highly significant. Both genes of the unequivocal plastid branch

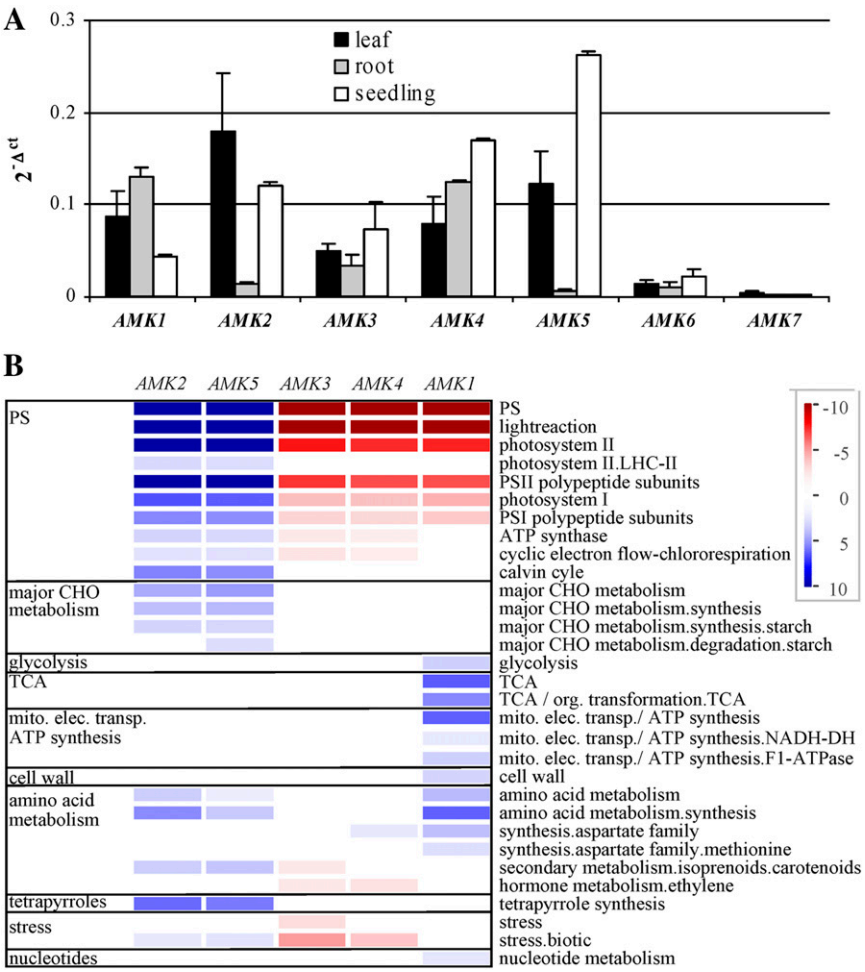

Figure 2. Expression and co-response analysis. A, Relative transcript levels of *AMK* genes. Rosette leaves of 21-d-old plants on soil, separate roots, or complete 16-d-old seedlings on plates containing one-half-strength MS with 0.5% Suc were analyzed by quantitative real-time RT-PCR. Values are expressed as difference of the ct value to *EF1α* taken to the power of efficiency. Each bar represents the mean values ± SD of three individual seedlings; measurements were repeated twice. B, Co-response analysis of *AMK* genes. The Arabidopsis co-response database was searched for transcriptional correlations using the nonparametric Spearman's Rho rank correlation and Bonferroni correction with the complete AtGenExpress developmental series in wild-type plants (http://csbdb.mpimp-golm.mpg.de; atge0100: developmental series [only WT]). Visualization was done with MapMan (http://gabi.rzpd.de/projects/MapMan) together with PageMan (http://mapman.mpimp-golm.mpg.de/pageman) and statistical analysis of Wilcoxon's test, including the correction of multiple testing by Bonferroni. *P* values were assigned a positive or negative value, depending on whether the correlation was positive or negative, with increasing blue and red indicating an increasingly and decreasingly significant correlation, respectively. All significant MapMan categories of metabolic processes that match our high stringent selection are shown.

(*AMK2* and *AMK5*) showed identical expression correlations. Both genes of the probable cytosol branch (*AMK3* and *AMK4*) also showed identical expression correlations; however, expression correlations of the plastid and the probable cytosol branch were obviously significantly different. This may lead to the speculation that adenylate kinases are redundant in their respective compartment. Interestingly, no correlated expressions were found with genes involved in nucleotide biosynthesis, although expression of genes involved in pyrimidine and purine de novo synthesis are coregulated to some extent (Giermann et al., 2002; van der Graaff et al., 2004).

Based on phylogenetic studies and the expression co-response analysis, we focused on the functional characterization of highly expressed plastidic adenylate kinases. For this purpose, we used two independent T-DNA insertion lines for the characterization of *AMK2* and one line for the characterization of *AMK5* (Fig. 3A). The structure of genes and regions of homology between both sequences demonstrate that the C terminus of AMK5 extends that of AMK2 by 290 amino acids. To date, no indication has been found of a possible function of this C-terminal domain.

Isolation of Mutants

Plants with insertions in *AMK5* (SALK_000200) or *AMK2* (SALK_031816, GABI-KAT_034C05) were obtained from the Salk collection (Alonso et al., 2003) and the GABI-KAT services (Rosso et al., 2003). Using combinations of gene-specific and T-DNA-specific oligonucleotides, the presence of T-DNA inserts was confirmed using PCR (data not shown). Heterozygous T-DNA insertions in *AMK2* were identified from SALK_031816 (*Amk2-1*) and GABI-KAT_034C05 (*Amk2-2*) that did not show differences from wild types. Developing siliques of heterozygous parents contained approximately 25% pale and approximately 75% green seeds (Fig. 3B). Embryos dissected out of these seeds had a pale green to white color (Fig. 3B). Both putative *amk2* mutants showed the same whitish seed phenotype. The seed coat was separated, and genotyping of the embryonic tissue confirmed that the whitish embryos are indeed homozygous *amk2* mutants, whereas the green embryos segregate into heterozygous mutants and wild types (Fig. 3C). Interallelic crosses of heterozygous *amk2-1* with heterozygous *amk2-2* plants demonstrated that the white embryo segregation is

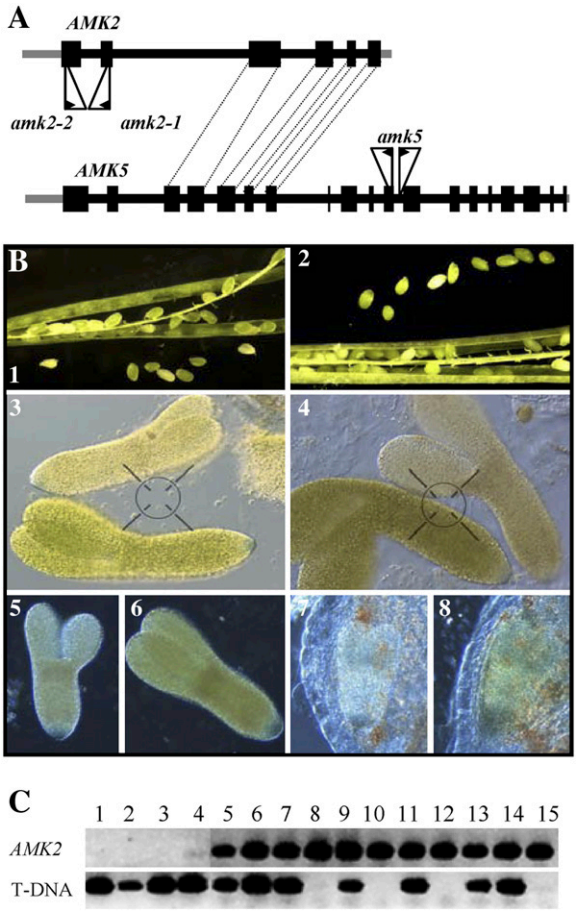

Figure 3. Phenotype of *amk2* mutant seeds. A, Structure of Arabidopsis *AMK2* and *AMK5*. Gray lines indicate 5′-untranslated regions, black boxes indicate exons, and black lines are introns. Exons with high similarity are connected with dotted lines. White triangles indicate the position of the T-DNA insertion sites of *amk2-1* (Salk_031816), *amk2-2* (Gabi-Kat_034C05), and *amk5* (Salk_000200). Salk_000200 contains two inserted T-DNAs, 129 bp apart from each other. B, Seeds and embryos. 1, *AMK2-1/amk2-1* silique 10 d after flowering (DAF); 2, *AMK2-1/amk2-1* silique 14 DAF; 3, *AMK2-1/amk2-1* dissected embryos; 4, *AMK2-2/amk2-2* dissected embryos; 5 and 6, F_2 embryos in late torpedo state from *AMK2-2/amk2-2* × *AMK2-1/amk2-1*; 7 and 8, F_2 embryos in early torpedo state from *AMK2-2/amk2-2* × *AMK2-1/amk2-1*. C, Genotype of dissected embryos (14 DAF) of an *AMK2-1/amk2-1* plant; lanes 1 to 4, white seeds, lanes 5 to 15, green seeds.

maintained in F_1 seed populations (green:white seeds 3:1; data not shown). The fact that the two independent *amk2* alleles behave identically and the segregation of the phenotype prove that the observed phenotype is caused by disruptions of *AMK2*.

Seeds from heterozygous plants that contain homozygous *amk2* mutant embryos develop into slightly wrinkled seeds (data not shown). These seeds germinate and grow heterotrophically on medium containing Suc. The rescued homozygous *amk2* seedlings were bleached and strongly retarded in growth compared to heterozygous mutants or wild types (Fig. 4A). Under photoautotrophic conditions, both allelic *amk2* mutations were lethal. For all experiments, the offspring of heterozygous *Amk2* plants was used.

Homozygous *amk5* mutants were isolated from a selfed population of SALK_000200. In comparison to wild types, no obvious growth or developmental differences were observed (Fig. 4B).

Transcripts of *AMK2* and *AMK5* Are Absent in the Respective T-DNA Insertion Lines

To determine whether the T-DNA insertion reduces the respective transcript level, quantitative real-time RT-PCR was performed. As shown in Figure 5, virtually no *AMK2* or *AMK5* transcripts were detected in the respective mutant seedlings, thus confirming that *amk2* and *amk5* mutants can be regarded as complete knockout for the respective gene product.

To establish whether absence of either *AMK2* or *AMK5* expression results in altered transcript profiles for other genes involved in nucleotide metabolism, all genes of purine de novo synthesis, adenine recycling, and nucleotide phosphotransfer were analyzed. With the exception of *PurE2* and *APT4*, all genes could be detected in 16-d-old, heterotrophically grown wild types (Supplemental Fig. S1). Although *amk2* mutants show a rather severe phenotype, the differences observed for the tested transcript levels are considerably low (Fig. 5). Nevertheless, there is significantly reduced expression of genes involved in purine de novo synthesis (*PurA*, *PurB*, *PurC*, *PurL*, and *PurM*). Although *amk5* mutants show no phenotype, there is significantly increased expression of genes involved in adenine salvage (*Apt1* to *Apt5*, and *Adk1* and *Adk2*). Also, the *PRS* genes, responsible for supplying

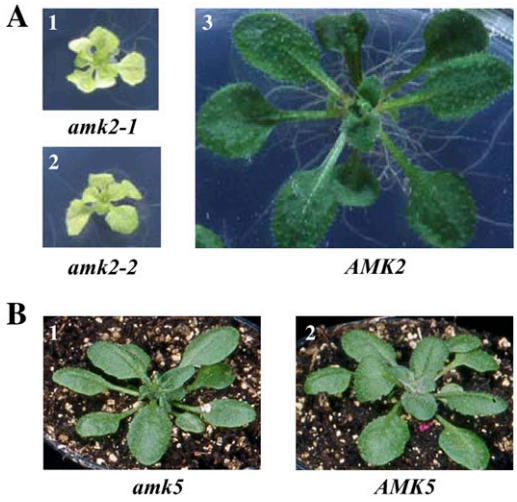

Figure 4. Phenotype of *amk* mutant plants. A, Growth phenotype of *amk2* mutant plants; 1, a*mk2-1/amk2-1*; 2, *amk2-2/amk2-2*; 3, *AMK2-2/amk2-2*. Plants were grown for 21 d on plates containing one-half-strength MS with 0.5% Suc. Pictures were taken with the same magnification. B, Growth phenotype of *amk5* mutant plants; 1, a*mk5/amk5*; 2, *AMK5/amk5*. Plants were grown for 4 weeks on soil. Pictures were taken with the same magnification.

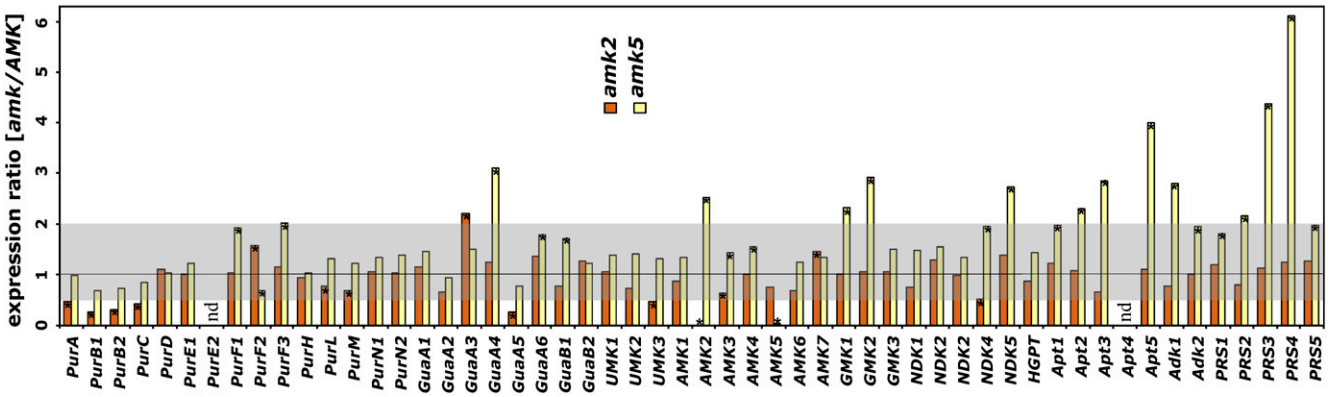

Figure 5. Relative transcript levels of nucleotide metabolism genes in *amk* mutants. Sixteen-day-old seedlings grown on plates containing one-half-strength MS with 0.5% Suc were analyzed by quantitative real-time RT-PCR. Values are calculated as the difference of the ct value to *UBQ-10* taken to the power of efficiency. Each bar represents the expression of the gene of question in the respective mutant to the expression of the wild type. Each bar represents the mean values ± SE of three to five individual seedlings. Measurements were repeated twice. The gray bar shades differences that are less than 2-fold. *PurA*, Adenylosuccinate synthetase EC 6.3.4.4; *PurB*; adenylosuccinate lyase EC 4.3.2.2; *PurC*; SAICAR synthase EC 6.3.2.6; *PurD*, GAR synthase EC 6.3.4.13; *PurE*, AIR carboxylase and N5CAIR mutase EC 4.1.1.21; *PurF*, PRPP amidotransferase EC 2.4.2.14; *PurH*, ACAR transforylase EC 2.1.2.3 and IMP cyclohydrolase EC 3.5.4.10; *PurL*, FGAM synthase EC 6.3.5.3; *PurM*, AIR synthase EC 6.3.3.1; *PurN*, GAR transformylase EC 2.1.2.2; *GuaA*, GMP synthase EC 6.3.5.2; *GuaB*, IMP dehydrogenase EC 1.1.1.205; *UMK*, UMP kinase EC 2.7.4.4; AMK, AMP kinase EC 2.7.4.3; *GMK*, GMP kinase EC 2.7.4.8; *NDK*, nucleoside diphosphate kinase EC 2.7.4.6; *HGPT*, hypoxanthine guanine phosphoribosyltransferase EC 2.4.2.8; *APT*, adenine phosphoribosyl transferase EC 2.4.2.7; *ADK*, adenosine kinase EC 2.7.1.20; *PRS*, PRPP synthetase EC 2.7.6.1. nd, Not detectable.

phosphoribosyl pyrophosphate (PRPP) for de novo and salvage reactions, are significantly induced. Conspicuously, there is a 2.5-fold increase of *AMK2* expression in *amk5* mutants.

AMK Activity Is Reduced in *amk2* But Not in *amk5*

To establish whether the absence of either *AMK2* or *AMK5* expression results in altered protein abundance, polyclonal antibodies were raised against AMK2. Although the amino acid sequences in the N-terminal regions of the predicted mature proteins are highly homologous, the antibody turned out to be specific for AMK2 and does not cross react with AMK5 protein overexpressed in *Escherichia coli* (data not shown). Rosette leaves of *amk2* plants contain no AMK2 protein (Fig. 6). Most striking is the increase of AMK2 protein in the *amk5* mutants, confirming the doubling of *AMK2* expression.

To provide evidence that AMK activities have been altered in the mutant lines, we measured total AMK activity of rosette leaves in both directions in heterotrophically grown *amk2*, *amk5*, and congenic wild types. Total adenylate kinase activity in *amk2* was reduced by 21% in the forward reaction and 37% in the backward reaction compared to wild types, when activity was calculated on total leaf protein basis (Table I). When calculated on a fresh weight (FW) basis, the reduction was a little more pronounced due to an altered protein to FW ratio in *amk2* (data not shown). Wild-type activities measured in both directions in rosette leaves of heterotrophically grown Arabidopsis seedlings were approximately 4.1 nkat (mg protein)$^{-1}$ and in agreement with previously reported values of tobacco (*Nicotiana tabacum*) leaf extracts (8.8 nkat [mg protein]$^{-1}$; Schlattner et al., 1996), but were more than 100 times higher than those reported for Arabidopsis by Carrari et al. (2005). Under any of the tested conditions, total extractable adenylate kinase activity measured in both directions was not changed in *amk5* mutants.

AMK5 Encodes AMK Activity

As the complete loss of *AMK5* transcript does not result in any reduction of AMK activity, it was tested whether *AMK5* really encodes adenylate kinase. Full-length proteins of AMK2 and AMK5 using pET-DEST42 constructs were overexpressed in *E. coli*, and protein induction was checked with His-tag specific antibodies (Fig. 7A). Production of AMK2 protein was always higher than AMK5. Purification of the His-tagged proteins proved to be impossible, as binding to nickel-nitrilotriacetic acid agarose could not be achieved under native conditions. Therefore, activity measurements

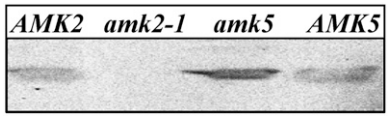

Figure 6. AMK2 specific protein levels in *amk* mutants. Immunoblot analysis of rosette leaves of 16-d-old seedlings grown on plates containing one-half-strength MS with 0.5% Suc. Size-fractionated proteins were immunodecorated with specific antiserum raised against AMK2. Congenic wild types (lanes 1 and 4), *amk2* mutant (lane 2), and *amk5* mutant (lane 3) are shown.

Table I. *Activity and nucleotide content in amk mutants*

Rosette leaves of seedlings were analyzed after 21 d of growth on plates containing one-half-strength MS with 0.5% Suc. Activity data are given as percentage of the controls, with forward reaction at 4.2 ± 1.3 nmol s^{-1} (mg protein)$^{-1}$ and backward reaction at 4.0 ± 1.5 nmol s^{-1} (mg protein)$^{-1}$. Each data point represents the mean and SD of seven replicates for *amk2*, nine replicates for congenic wild-type and heterozygous plants, and four replicates for *amk5*. Significant differences ($P < 0.1$) using unpaired two-tailed *t* tests are marked with an asterisk.

	amk2	*AMK*	*amk5*
Activity			
Forward reaction (% of control)	79 ± 15.7*	100 ± 19.2	99 ± 7.3
Backward reaction (% of control)	63 ± 14.9*	100 ± 4.3	101 ± 15.5
Metabolite content			
AMP (nmol g FW^{-1})	3.9 ± 1.8	5.4 ± 2.4	7.5 ± 1.0
ADP (nmol g FW^{-1})	8.5 ± 4.5*	25.5 ± 8.8	31.6 ± 2.0
ATP (nmol g FW^{-1})	18.7 ± 7.4*	50.4 ± 19.4	58.0 ± 10.1
Purine (nmol g FW^{-1})	32.8 ± 8.4*	89.5 ± 26.2	110 ± 15.9
Adenylate energy charge ([ATP] + [0.5 × ADP]) × ([ATP] + [ADP] + [AMP])$^{-1}$	0.72 ± 0.09*	0.79 ± 0.05	0.77 ± 0.03

were carried out with crude *E. coli* extracts together with control inductions. Total adenylate kinase activity of crude *E. coli* extracts was always higher in lines overexpressing AMK2 than in lines overexpressing AMK5, matching recombinant protein abundance (Fig. 7B). Independent of the variance in protein induction, there was always higher total AMK activity detectable in extracts that produced AMK2 or AMK5 compared to controls. This unequivocally demonstrates that both *AMK2* and *AMK5* encode adenylate kinase activity.

Adenine Nucleotide Pool Sizes in the Respective T-DNA Insertion Lines

Nucleotide levels were investigated in rosette leaves of heterotrophically grown *amk2*, *amk5*, and congenic wild types. In comparison to controls, homozygous *amk2* seedlings showed a significant reduction of total adenine nucleotides from 89.5 to 32.8 nmol (g FW)$^{-1}$ (Table I). Inspection of the individual adenine nucleotides revealed that there was a significant decrease of ATP and ADP and no change of AMP. Calculation of the adenylate energy charge showed a significant decrease in *amk2* plants. There is no change in nucleotide levels in plants in the absence of AMK5.

Chloroplast Ultrastructure of *amk2* Mutant Lines

The co-response analyses showed that *AMK2* transcription is coregulated with genes involved in photosynthesis, and the visual phenotype of *amk2* mutants resembles that of mutants disrupted in genes involved in photosynthesis or ''auxiliary'' processes (Maiwald et al., 2003; Bosco et al., 2004; Reiser et al., 2004). Therefore, the total chlorophyll content was measured, and imaging PAM (noninvasive chlorophyll fluorescence measurements) was used to analyze the primary photosynthetic processes in heterotrophically grown *amk2* and congenic wild types. As already obvious from Figure 3, the total chlorophyll content of *amk2* was strongly reduced (Table II). The quantum yield of PSII (Φ_{PSII}) was very low, while the nonphotochemical quenching (qN) was strongly increased in *amk2* mutants. Φ_{PSII} is an empirical index for the assessment of the effective PSII quantum yield, and qN is a complex phenomenon, summarizing components of state transition, photoinhibition, and energy quenching that reflects energy dissipated as heat related to the energetization of the thylakoid membrane.

We used antibodies raised against ATP synthase subunits atpF (subunit I of CF_O) and atpA (α-subunit of CF_1) to establish whether the ATP synthase complex is present in chloroplasts of *amk2* mutants. Both protein complex subunits were detectable in wild types and in heterozygous mutants, while homozygous

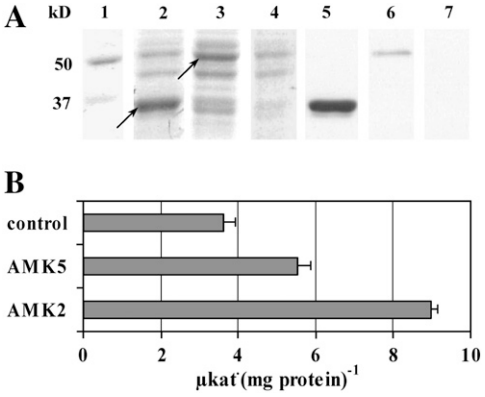

Figure 7. Analysis of recombinant AMK2 and AMK5 in *E. coli* lysates. A, Size-fractionated proteins of crude *E. coli* lysates 5 h after induction of the respective recombinant protein. Lanes 1 to 4, Coomassie staining of total proteins; lanes 5 to 7, immunoblot analysis with His-tag-specific antibody. Lane 1, Marker proteins; lanes 2 and 5, AMK2; lanes 3 and 6, AMK5; lane 4 and 7, control construct. Arrows indicate the AMK specific proteins of crude *E. coli* lysates. B, Adenylate kinase activity in crude *E. coli* lysates 5 h after induction. Total soluble protein extracts were measured in direction of ADP production (backward reaction). Data are the means and SD of three technical replicates of one representative induction.

Table II. *Photosynthesis parameter in amk mutants*

Rosette leaves of seedlings were analyzed after 21 d of growth on plates containing one-half-strength MS with 0.5% Suc. Φ_{PSII} and qN were determined using imaging PAM. The values were determined for three plants of the same genotype 5 min after the light (250 μmol photon m^{-2} s^{-1}) was switched on. Significant differences ($P < 0.1$) using unpaired two-tailed *t* tests are marked with an asterisk.

	amk2	*AMK*
Chlorophyll content (μg g FW^{-1})	13.6 ± 5.0*	412 ± 83.9
Φ_{PSII}	0.11 ± 0.011*	0.53 ± 0.040
qN	0.92 ± 0.018*	0.29 ± 0.018

amk2 mutants lacked significant amounts of these two subunits (Fig. 8A).

In addition, electron micrographs of wild-type, heterozygous, and homozygous *amk2* seedlings were prepared. Chloroplasts of heterozygous and wild-type seedlings showed typical sun-leaf morphology (Fig. 8B, 1). In contrast, chloroplasts of homozygous *amk2* mutants had generally lost the integrity of their thylakoid membrane structures and were very heterogeneous in their architecture. Many chloroplasts contained swollen grana thylakoids, whereas stroma thylakoids were rarely observed (Fig. 8B, 2 and 3). Very few examples of more intact chloroplasts could be found in *amk2* (Fig. 8B, 4). Most chloroplasts from homozygous *amk2* mutants were estimated to be 50% smaller than in heterozygous or wild-type plants. In addition, chloroplasts of homozygous *amk2* seedlings regularly showed an increased number of lipophilic plastoglobuli.

amk2 x *amk5* Double Mutants

To further investigate the function of AMK5, we created double mutants by intercrossing heterozygous *amk2* and homozygous *amk5* plants. Both genes are located on chromosome 5 with a genetic distance of approximately 27 cM between their loci. We determined the genotype of the F_3 offspring from the F_2 *amk5* x *AMK2-1/amk2-1* and *amk5* x *AMK2-2/amk2-2* plants. Both populations (209 and 208 seedlings, respectively) contained about 20% seedlings with a whitish *amk2*-like phenotype. PCR-based genotyping confirmed a Mendelian segregation for the *amk2* mutation (data not shown). The slight reduction from the expected 25% homozygous *amk2* mutants in the *amk5* background can be attributed to the severity of the *amk2* mutant phenotype and the weak genetic linkage of *AMK2* and *AMK5*. We did not find additional phenotypic characteristics in double mutants. Thus, no hypothesis of the putative function of AMK5 can be given yet.

DISCUSSION

There are only a few reports of the in planta function of specific adenylate kinase isoforms so far. Regierer et al. (2002) showed that the tuber-specific reduction of plastid adenylate kinase (*StpADK*) leads to an increase in the adenylate pool and increased starch content in potato tubers. A knockout Arabidopsis mutant defective in *AMK1*, the closest homolog to *StpADK*, had a contrasting phenotype, with decreased adenylates, elevated amino acid levels, and reduced starch content in roots but not in leaves (Carrari et al., 2005). In this study, we have classified the entire adenylate kinase gene family using phylogenetic analysis and gene expression correlations. Based on these findings, we addressed two further members of the *AMK* family that are located in plastids (*AMK2* and *AMK5*).

AMK2 Constitutes an Essential Fraction of Total AMK Activity

Stitt and coworkers found in their study using subcellular fractions of wheat (*Triticum aestivum*) pro-

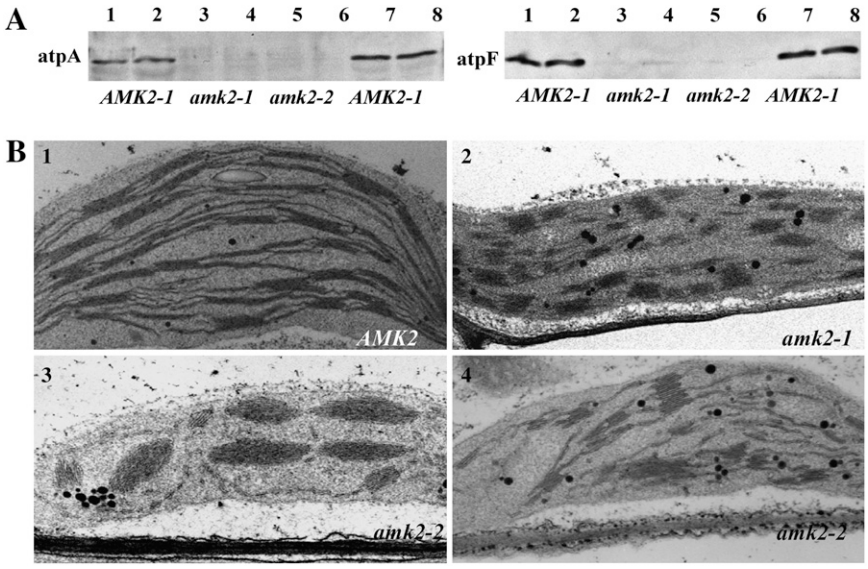

Figure 8. Photosynthesis-related analysis of *amk2* mutants. A western blot of rosette leaves of 16-d-old seedlings grown on plates containing one-half-strength MS with 0.5% Suc for ATP-synthase subunits. Size-fractionated proteins were immunodecorated with specific antiserum raised against the ATP-synthase subunit proteins as indicated. Lanes 1 and 8, wild types; lane 2, *AMK2-1/amk2-1*; lanes 3 and 4, *amk2-1/amk2-1*; lanes 5 and 6, *amk2-2/amk2-2*; lane 7, *AMK2-2/amk2-2*. B, Ultrastructure of chloroplasts from wild-type and *amk2* mutant plants. Electron micrographs of leaf tissues. 1, Wild type; 2, homozygous *amk2-1*; 3 and 4, two individual homozygous *amk2-2* plants. All pictures were taken with 16,000× magnification. The leaves were collected from 21-d-old plants grown on one-half-strength MS with 0.5% Suc.

toplasts that 56% of total adenylate kinase activity is in plastids, 3% in the cytosol, and 41% associated with mitochondria (Stitt et al., 1982). Other studies showed that 57% to 72% of total adenylate kinase activity in spinach (*Spinacia oleracea*) is associated with plastids (Birkenhead et al., 1982). Assuming comparable distribution of adenylate kinase activity in Arabidopsis reduction of only 30% in *amk2* mutants would eliminate approximately 38% to 51% of the plastid-associated adenylate kinase activity. Plastid adenylate kinase activity is not exclusively located within the stroma but is also bound to envelope membranes of spinach (Murakami and Strotmann, 1978). Up to now, it was not known whether substantial amounts of plastid-associated adenylate kinase were not inside the stroma of Arabidopsis. Targeting of stably transformed GFP-fusions and subcellular proteome analysis (Peltier et al., 2006), together with the severe phenotype of *amk2* mutants, demonstrated that AMK2 forms an essential fraction of stromal adenylate kinase. Furthermore, subcellular proteome analysis has found an association of AMK5 with the thylakoid and envelope fraction of plastids (Peltier et al., 2004). Together with the unaltered phenotype of *amk5* mutants and the fact that AMK5 cannot substitute the loss of AMK2, it is postulated that AMK5 activity is not located in the chloroplast stroma.

AMK2 Is Important for Chloroplast Integrity

Loss of AMK2 leads to an altered architecture of chloroplasts. This does not prevent embryo development and germination. Similar phenotypes have been observed with mutants in photosynthesis proteins (Maiwald et al., 2003; Bosco et al., 2004), and related phenotypes have been found in purine biosynthesis mutants (Hung et al., 2004; van der Graaff et al., 2004). Functional chloroplasts become crucial after germination when seedlings have to grow independently from resources of the seed storage organs. Mutant *amk2* cannot grow autotrophically and show impaired growth even in the presence of sugars and low light. In contrast, mutants in ATP synthase subunits or the Rieske protein are all seedling lethal but are able to survive with exogenous sugar and in low light (Maiwald et al., 2003; Bosco et al., 2004).

It was shown that two important subunits of the ATP synthase are not detectable in *amk2*. The loss of functional plastid ATP synthase is in agreement with a block of the photosynthetic electron transport chain of *amk2*, indicated by high qN. This correlates with low abundance of stroma thylakoids, the major location of ATP synthase. Grana thylakoids were present in *amk2* mutants but were strongly swollen. From these observations, one might speculate that AMK2 is important for the photosynthetic electron flow by supplying the major part of ADP substrate to the ATP synthase complex. However, it is also likely that the severe chloroplast phenotype is an indirect result of the inability of the chloroplast to equilibrate its adenylates. This is supported by the impossibility to rescue *amk2* seedlings by feeding with adenosine or IMP (Supplemental Fig. S2), while mutants in purine biosynthesis could be complemented by feeding nucleotide precursors (Hung et al., 2004; van der Graaff et al., 2004).

Loss of AMK2 Leads to Disruption of the Adenine Nucleotide Pool

Nucleotide measurements showed that *amk2* mutants have a reduced adenine nucleotide pool. These results indicate that disruption of *AMK2* interferes with de novo synthesis of adenine nucleotides. Furthermore, a decrease of the adenylate energy charge was found. It has to be considered that these measurements include metabolites from plastids, the cytosol, and mitochondria. In mature leaves, approximately one-half of the adenylate pool is present in the plastids, 40% in the cytosol, and the remainder in mitochondria (Stitt et al., 1982). Our data locate AMK2 in the chloroplasts, and other members of the AMK family are presumably responsible for the equilibration of adenylate pools outside the plastid. It is therefore possible that the disturbance of the adenine nucleotides in *amk2* is larger in plastids than indicated by our measurements of whole leaf extracts. Subcellular fractionation would be required to confirm this possibility but was not possible due to the small amounts of tissue available from *amk2* mutants.

Several observations support the hypothesis that most ATP necessary for plastid-generated metabolites (such as nucleotides, lipids, or amino acids) is produced within the plastid. Most enzymes involved in the purine de novo synthesis are located in plastids (Moffatt and Ashihara, 2002; Boldt and Zrenner, 2003; van der Graaff et al., 2004; Zrenner et al., 2006). Metabolite flux analyses demonstrated that plastids from developing rapeseed (*Brassica napus*) embryos do not require ATP import to achieve high rates of lipid biosynthesis (Schwender et al., 2004). The identified plastidic nucleotide uniporter is proposed to function as nucleotide exporter of plastids (Leroch et al., 2005), and the two known plastid ATP/ADP translocators presumably supply ATP only to storage plastids (Schünemann et al., 1993; Neuhaus and Emes, 2000) or are required to import ATP in the dark when the major source of ATP is oxidative phosphorylation in mitochondria (Reinhold et al., 2007). The fact that *amk2* embryos fully develop and mature seeds germinate indicates that structural metabolites needed in the early phases of development are likely to be synthesized with the help of cytosolic and mitochondrial ATP pools. During embryo formation and predominantly during embryo germination, salvage processes exceed nucleotide de novo synthesis (Stasolla et al., 2003). While de novo synthesis is largely located in plastids, salvage pathways take place in the cytosol. The severe phenotype of the *amk2* mutants indicates that cytosolic nucleotide pools are not able to fully compensate loss of AMK2.

AMK5 Is Not Essential

The complete loss of *AMK5* transcript does not result in reduction of total AMK activity or any visible phenotype, indicating that AMK5 is nonessential or redundant with other adenylate kinases. The disruption of *AMK5* is alleviated by the doubling of *AMK2* expression and increasing AMK2 protein, demonstrating that other AMK activities can compensate loss of AMK5. This is in agreement with the fact that we were able to obtain *amk2* x *amk5* double mutants with no additional phenotypic characteristics. Both AMK2 and AMK5 show adenylate kinase activity and comparable transcript profiles in young embryos (Spencer et al., 2007) and throughout development. Preliminary results with overexpressed proteins in crude *E. coli* extracts gave no hint about big differences in substrate specificities (data not shown). In this respect, it is interesting to note that AMK5 has an additional C-terminal domain with no apparent similarity to other proteins or protein patterns. Because subcellular proteome studies have found AMK5 in the thylakoid- and envelope-associated fractions (Froehlich et al., 2003; Peltier et al., 2004), it is postulated that this protein is not located in the plastid stroma.

CONCLUSION

Adenylate kinases equilibrate adenylates by reversible formation of ADP through transfer of one phosphate group from ATP to AMP. Adenylate kinase activity is encoded by a gene family in Arabidopsis. Functional analysis using T-DNA insertion mutants revealed that only one member of the adenylate kinase gene family is important for equilibration of adenylates and de novo synthesis of ADP in the plastid stroma.

MATERIALS AND METHODS

Plant Materials and Growth Conditions

Arabidopsis (*Arabidopsis thaliana*) Columbia-0, SALK_031816 (*amk2-1*), and SALK_000200 (*amk5*) were obtained from Nottingham Arabidopsis Stock Centre (University of Nottingham, Loughborough, UK), and GABI_300A04 (*amk2-2*) was obtained from the GABI-Kat collection (Max-Planck-Institut für Züchtungsforschung, Cologne, Germany). Seeds were surface sterilized and aseptically grown on media containing one-half strength Murashige and Skoog (MS) salts, 0.25 mM MES, pH 5.7 (KOH), 0.5% (w/v) Suc, and 0.7% (w/v) agar. Seeds were imbibed at 5°C in darkness for 48 h and grown in a 12-h photoperiod (photon flux density, 150 μmol m^{-2} s^{-1}; 22°C light, 18°C dark). Plants on soil were grown in a 16-h photoperiod (photon flux density, 120 μmol m^{-2} s^{-1}; 60% relative humidity, 20°C light, 18°C dark).

Construction of Fusion Proteins

The entire open reading frames of *AMK*s were amplified from first-strand cDNA by PCR with *Pfu*-polymerase (MBI Fermentas) using the following oligonucleotides: amk1_5, CACCATGGCGAGATTAGTGCGTGT; amk1_3, TGCTGCGACAGACTGTTTCTC; amk2_5, CACCATGACGGGCTGTGTGAATTC; amk2_3, ACTTAAAAGTGAACTTGGAGCAGTG; amk3_5, CACCATGGCAACGAGCAGTGC; amk3_3, TGTAGACACAACCTTCTTCACCAC; amk5_5, CACCATGGCGTCTCTTTCTCTCAGTTC; amk5_3, CGAAAACACGCTACTCAAGAACC; amk7_5, CACCATGGCCTGGCTTAGCCG; and amk7_3, GAAAAGTACCTCCTGTGCGTAGACA.

PCR products were inserted into entry vector PENTR/SD/D-TOPO according to the manufacturer's instructions (Invitrogen). For sequence confirmation, positive entry clones were sequenced (MWG Biotech). Clones were recombined into pK7FWG2 plant transformation vector for C-terminal GFP-fusion (Karimi et al., 2002) and into pET-DEST42 (Invitrogen) for C-terminal His-fusion using the Gateway LR-Clonase (Invitrogen). Binary vectors were transferred into Arabidopsis plants by *Agrobacterium*-mediated infiltration (Clough and Bent, 1998). Transgenic plants were selected by kanamycin resistance. Confocal microscopy was performed on 4- to 6-week-old plants grown on soil. For the transient expression of the DHODH-DsRed fusion protein (pUC vector containing 35S promoter-driven expression construct of the first 80 amino acids of dihydroorotate dehydrogenase of tobacco [*Nicotiana tabacum*] [Giermann et al., 2002] fused to DsRed [CLONTECH]), 5- to 6-week-old leaves were bombarded with the Biolistic PDS-1000/He particle delivery system (Bio-Rad). Bombarded plant leaves were incubated in petri dishes containing wet filter paper, and confocal microscopy was carried out 2 to 3 d later. For transient expression of AMK7 C-terminal GFP-fusion proteins, PEG-mediated transfection of Arabidopsis protoplasts was performed (Yoo et al., 2007), and confocal microscopy was carried out 2 d later.

Bioinformatic Analyses

Gene and protein sequences were obtained from The Arabidopsis Information Resource (www.arabidopsis.org) and the National Center for Biotechnology Information (www.ncbi.nlm.nih.gov) using homology (BLAST) searches. Sequence comparisons were done with ClustalW software (www.ebi.ac.uk/clustalW). For analysis of evolutionary relationships, we exploited the conserved domain database cdd (www.ncbi.nlm.nih.gov/Structure/cdd) with cd01428 ADK using CDTree (www.ncbi.nlm.nih.gov/Structure/cdtree). For predicting intracellular localization of mature proteins, the software packages Target P1.1 (www.cbs.dtu.dk/services/TargetP/; Emanuelsson et al., 2007), iPSORT (biocaml.org/ipsort/iPSORT/; Bannai et al., 2002), and Predotar 1.03 (urgi.versailles.inra.fr/predotar/predotar.html; Small et al., 2004) were used. The protein sequences of *AMK2* and *AMK5* were aligned with Align (www.ebi.ac.uk/Align) set to needle with an EPAM100 Matrix.

For transcriptional correlation analysis, we used the Arabidopsis coresponse database (csbdb.mpimp-golm.mpg.de; Steinhauser et al., 2004) with the visualization tools MapMan (http://gabi.rzpd.de/projects/MapMan; Thimm et al., 2004; Usadel et al., 2005) and PageMan (http://mapman.mpimp-golm.mpg.de/pageman; Usadel et al., 2006).

Microscopy

For the localization of GFP-fusions, a confocal microscope system (Leica and Leica Confocal Software LCS) was used. Pictures of dissected siliques and embryos were taken using a SPOT-RT camera (Visitron) attached to an Olympus Systemmicroscope BX41TF (Olympus) controlled by the MetaVue software package (Visitron).

For electron microscopy, pieces of 2 mm^2 from rosette leaves were fixed for 2 h with 2.5% (v/v) glutaraldehyde in 0.1 M sodium-potassium phosphate, pH 7.0, including 2% (w/v) paraformaldehyde and 0.05% (w/v) tannic acid. After washing with phosphate buffer, samples were incubated for 12 h in 50 mM sodium-potassium phosphate, pH 7.0, containing 1% (w/v) osmium tetroxide. After washing with phosphate buffer, the samples were dehydrated in a graded series of ethanol, followed by propylene oxide, incubated in a mixture of propylene oxide/ERL (v/v) and pure ERL (Spurr, 1969), and polymerized overnight at 60°C. Ultrathin sections were contrasted with uranyl acetate and lead citrate. Transmission electron micrographs were obtained with a Siemens 101 at 80 kV. The negatives were scanned with an Epson 1680 Pro Scanner at 1,200 dpi.

DNA Isolation and Mutant Screening

Screening and selection within the mutant population was done following the Signal Salk/GABI-Kat instructions (www.signalsalk.edu and www.mpiz-koeln.mpg.de/GABI-Kat/General_Information). For genotyping, a small leaf or a single dissected embryo and the following oligonucleotides were used: S_031816 L, CCAAATTTCAGGTGAATGATTGT; S_031816R, GCTATAAGTGGCCGAGTTAAGGT; G_034C05L, AAATACCAAATGCAAACGAATAGG; G_034C05R, CGATAATCGACGGAGATCTTGATA; S_000200 L, GTTTACCGGATAGGAACCTTGAT; S_000200R, GATATTTACCAATTGCACCAAGC; GABI_R, CCAAAGATGGACCCCCACCCAC; and SALK_LBb1, GCGTGGACCGCTTGCTGCAACT.

All measurements were carried out with plants of the fourth or fifth generation.

RNA Isolation and Transcript Detection

Total RNA was isolated using the NucleoSpin plant kit (Macherey & Nagel), including an on-column DNaseI digestion. For quantitative real-time RT-PCR, complete 16-d-old sterile, culture-grown seedlings were used.

For real-time RT-PCR, single-stranded cDNA synthesis was carried out with total RNA using SuperScript III RNase H^- reverse transcriptase (Invitrogen). Quantitative two-step RT-PCR was performed using the SYBR Green 1 protocol (Wittwer et al., 1997) and a 7900HT fast real-time PCR system (Applied Biosystems). The oligonucleotides are listed in Supplemental Table S1.

Recombinant Protein Expression in *Escherichia coli*

Overexpression in *E. coli* and His-tagged purification of recombinant proteins were done using standard procedures (QIAexpressionist; Qiagen), with the exception that induction was performed at 20°C. Denaturing purification was used to isolate AMK2. Antibodies were produced in rabbits by Eurogentec. Native isolation was applied for activity measurements. As control, pET-DEST42 was used containing a 370-bp fragment of β-lactamase that does not encode any peptide sequence.

Analysis of Enzyme Activities

Frozen plant material was ground in liquid nitrogen using a ball-mill. Then 10- to 20-mg aliquots were extracted by vortexing with 50 to 200 μL of extraction buffer. Composition of extraction buffer was 100 mM Tricine, pH 7.8 (KOH), 10% (v/v) glycerol, 0.1% (v/v) Triton X-100, 5 mM $MgCl_2$, 1 mM EDTA, 1 mM EGTA, 1 mM phenylmethylsulfonyl fluoride, 1 mM benzamidine, 1 mM ε-aminocaproic acid, and 5 mM dithiothreitol. Extracts were centrifuged at 16,000*g*, 10 min, 4°C. Measurement was performed in microplates by mixing 2 μL of extract supernatant with 100 μL of measuring buffer following the protocols of Kleczkowski and Randall (1986) for assaying adenylate kinase reaction in direction of ATP and AMP formation (forward) and in direction of ADP production (backward).

Western-Blot Analysis

Proteins were extracted with homogenization buffer containing 150 mM Tris-HCl, pH 7.5, 10 mM KCl, 10% (v/v) glycerol, 0.01% Triton X-100, and 1 mM β-mercaptoethanol. Extracts were centrifuged at 15,000*g*, 10 min, 4°C. After quantification, 10 μg of each extract was subjected to SDS-PAGE (12%). For immunodetection, proteins were transferred to Immobilon-P membranes (Millipore) by semidry electroblotting (Bio-Rad). The membranes were incubated with antisera raised against AMK2 protein or thylakoid membrane proteins (generously provided by J. Meurer, Ludwig-Maximilians University, Munich), and signals were detected using secondary antibody alkaline phosphatase conjugates and NBT/BCIP (Sigma) as substrate. For detection of His-tags, the INDIA-HisProbe-HRP (Pierce) and chemiluminescence detection were used.

Noninvasive Chlorophyll Fluorescence Measurement

Chlorophyll fluorescence measurements were performed using pulse amplitude modulated fluorometer PAM (2000) interfaced with the data acquisition system (Pamwin; Walz). Leaves were dark adapted for 20 min prior to induction fluorescence measurements. Minimal (F_o) and maximal (F_m) fluorescence, F_m in the light (F_m'), steady-state fluorescence immediately prior to the flash (F_t), and the ratio ($[F_m' - F_t]/F_m'$) reflecting the Φ_{PSII} (Maxwell and Johnson, 2000) were recorded at 20°C. qN was determined as $1 - (F_m' - F_o)/(F_m - F_o)$ (Kooten and Snel, 1990). The intensity of saturating light flashes (800 ms) used for detection of F_m' was 4,000 μmol photon m^{-2} s^{-1}, and actinic light intensity was 250 μmol photon m^{-2} s^{-1}. Chlorophyll content was measured according to Arnon (1949).

Metabolite Analysis

Plant material was quickly frozen in liquid nitrogen and extracts were made using the trichloroacetic acid procedure (Jelitto et al., 1992). Metabolites were measured as done by Schröder et al. (2005). A spectrophotometric assay was used to quantify AMP (Stitt et al., 1989).

Supplemental Data

The following materials are available in the online version of this article.

Supplemental Figure S1. Relative transcript levels of nucleotide metabolism genes.

Supplemental Figure S2. Growth of *amk2* with adenosine and IMP.

Supplemental Table S1. Oligonucleotides used for real-time RT-PCR.

ACKNOWLEDGMENTS

We thank the Nottingham Arabidopsis Stock Centre (NASC) and German Plant Genomics Program (GABI-Kat) for seeds. The authors thank J. Meurer (Ludwig-Maximilians Universität, Munich) for providing antibodies against atpA and atpF, J. Fisahn (Max-Planck-Institut für Molekulare Pflanzenphysiologie, Golm, Germany) for providing assistance with the chlorophyll fluorescence analysis, B. Usadel (Max-Planck-Institut für Molekulare Pflanzenphysiologie, Golm, Germany) for help with gene expression correlations, F. Kaulbars (Freie Universität Berlin, Institut für Biologie, Berlin) for help with electron microscopy, and M. Stitt (Max-Planck-Institut für Molekulare Pflanzenphysiologie, Golm, Germany) for critically reading the manuscript and the very helpful discussions.

Received December 7, 2007; accepted December 21, 2007; published December 27, 2007.

LITERATURE CITED

Alonso JM, Stepanova AN, Leisse TJ, Kim CJ, Chen H, Shinn P, Stevenson DK, Zimmerman J, Barajas P, Cheuk R, et al (2003) Genome-wide insertional mutagenesis of Arabidopsis thaliana. Science **301:** 653–657

Arnon GI (1949) Copper enzymes in isolated chloroplasts. Plant Physiol **24:** 1–15

Atkinson DE (1968) The energy charge of the adenylate pool as a regulatory parameter. Interaction with feedback modifiers. Biochemistry **7:** 4030–4034

Bannai H, Tamada Y, Maruyama O, Nakai K, Miyano S (2002) Extensive feature detection of N-terminal protein sorting signals. Bioinformatics **9:** 298–305

Birkenhead K, Walker D, Foyer CH (1982) The intracellular distribution of adenylate kinase in the leaves of spinach, wheat and barley. Planta **156:** 171–175

Boldt R, Zrenner R (2003) Purine and pyrimidine biosynthesis in higher plants. Physiol Plant **117:** 297–304

Bomsel JL, Pradet A (1968) Study of adenosine 5′-mono-,di- and triphosphates in plant tissues. IV. Regulation of the level of nucleotides, in vivo, by adenylate kinase: theoretical and experimental study. Biochim Biophys Acta **162:** 230–242

Bosco CD, Lezhneva L, Biehl A, Leister D, Strotmann H, Wanner G, Meurer J (2004) Inactivation of the chloroplast ATP synthase gamma subunit results in high non-photochemical fluorescence quenching and altered nuclear gene expression in Arabidopsis thaliana. J Biol Chem **279:** 1060–1069

Buchanan JM, Hartmann SC (1959) Enzymatic reactions in the synthesis of purines. Adv Enzymol Relat Areas Mol Biol **21:** 199–216

Carrari F, Coll-Garcia D, Schauer N, Lytovchenko A, Palacios-Rojas N, Balbo I, Rosso M, Fernie AR (2005) Deficiency of a plastidial adenylate kinase in Arabidopsis results in elevated photosynthetic amino acid biosynthesis and enhanced growth. Plant Physiol **137:** 70–82

Chapman AG, Fall L, Atkinson DE (1971) Adenylate energy charge in Escherichia coli during growth and starvation. J Bacteriol **108:** 1072–1086

Cheek S, Zhang H, Grishin NV (2002) Sequence and structure classification of kinases. J Mol Biol **320:** 855–881

Christopherson RI, Szabados E (1997) Nucleotide biosynthesis in mammals. *In* L Agius, HAS Sherratt, eds, Channeling in Intermediary Metabolism. Portland Press, London, pp 315–335

Clough SJ, Bent AF (1998) Floral dip: a simplified method for *Agrobacterium*-mediated transformation of *Arabidopsis thaliana*. Plant J **16:** 735–743

Duchene AM, Giritch A, Hoffmann B, Cognat V, Lancelin D, Peeters NM, Zaepfel M, Marechal-Drouard L, Small ID (2005) Dual targeting is the rule for organellar aminoacyl-tRNA synthetases in *Arabidopsis thaliana*. Proc Natl Acad Sci USA **102:** 16484–16489

Emanuelsson O, Brunak S, von Heijne G, Nielsen H (2007) Locating proteins in the cell using TargetP, SignalP, and related tools. Nat Protoc **2:** 953–971

Farre EM, Tiessen A, Roessner U, Geigenberger P, Tretheway RN, Willmitzer L (2001) Analysis of the compartmentation of glycolytic intermediates, nucleotides, sugars, amino acids and sugar alcohols in potato tubers using a non-aqueous fractionation method. Plant Physiol **127:** 685–700

Froehlich JE, Wilkerson CG, Ray WK, McAndrew RS, Osteryoung KW, Gage DA, Phinney BS (2003) Proteomic study of the Arabidopsis thaliana chloroplastic envelope membrane utilizing alternatives to traditional two-dimensional electrophoresis. J Proteome Res **2:** 413–425

Geigenberger P, Stitt M (2000) Diurnal changes in sucrose, nucleotides, starch synthesis and AGPS transcript in growing potato tubers that are suppressed by decreased expression of sucrose phosphate synthase. Plant J **23:** 795–806

Giege P, Heazlewood JL, Roessner-Tunali U, Millar AH, Fernie AR, Leaver CJ, Sweetlove LJ (2003) Enzymes of glycolysis are functionally associated with the mitochondrion in *Arabidopsis* cells. Plant Cell **15:** 2140–2151

Giermann N, Schröder M, Ritter T, Zrenner R (2002) Molecular analysis of *de novo* pyrimidine synthesis in solanaceous species. Plant Mol Biol **50:** 393–403

Hampp R, Goller M, Ziegler H (1982) Adenylate levels, energy charge, and phosphorylation potential during dark-light and light-dark transition in chloroplasts, mitochondria, and cytosol of mesophyll protoplasts from *Avena sativa* L. Plant Physiol **69:** 448–455

Heazlewood JL, Tonti-Filippini JS, Gout AM, Day DA, Whelan J, Millar AH (2004) Experimental analysis of the *Arabidopsis* mitochondrial proteome highlights signaling and regulatory components, provides assessment of targeting prediction programs, and indicates plant-specific mitochondrial proteins. Plant Cell **16:** 241–256

Hung WF, Chen LJ, Boldt R, Sun CW, Li HM (2004) Characterization of Arabidopsis glutamine phosphoribosyl pyrophosphate amidotransferase-deficient mutants1. Plant Physiol **135:** 1314–1323

Igamberdiev AU, Kleczkowski LA (2006) Equilibration of adenylates in the mitochondrial intermembrane space maintains respiration and regulates cytosolic metabolism. J Exp Bot **57:** 2133–2141

Jelitto T, Sonnewald U, Willmitzer L, Hajirezeai M, Stitt M (1992) Inorganic pyrophosphate content and metabolites in potato and tobacco plants expressing *E coli* pyrophosphatase in their cytosol. Planta **188:** 238–244

Karimi M, Inze D, Depicker A (2002) GATEWAY vectors for Agrobacterium-mediated plant transformation. Trends Plant Sci **7:** 193–195

Kleczkowski LA, Randall DD (1986) Maize leaf adenylate kinase: purification and partial characterization. Plant Physiol **81:** 1110–1114

Kooten O, Snel JFH (1990) The use of chlorophyll fluorescence nomenclature in plant stress physiology. Photosynth Res **25:** 147–150

Leroch M, Kirchberger S, Haferkamp I, Wahl M, Neuhaus HE, Tjaden J (2005) Identification and characterization of a novel plastidic adenine nucleotide uniporter from Solanum tuberosum. J Biol Chem **280:** 17992–8000

Maiwald D, Dietzmann A, Jahns P, Pesaresi P, Joliot P, Joliot A, Levin JZ, Salamini F, Leister D (2003) Knock-out of the genes coding for the Rieske protein and the ATP-synthase delta-subunit of Arabidopsis effects on photosynthesis, thylakoid protein composition, and nuclear chloroplast gene expression. Plant Physiol **133:** 191–202

Maxwell K, Johnson GN (2000) Chlorophyll fluorescence: a practical guide. J Exp Bot **51:** 659–668

Millar AH, Sweetlove LJ, Giege P, Leaver CJ (2001) Analysis of the Arabidopsis mitochondrial proteome. Plant Physiol **127:** 1711–1727

Millar AH, Whelan J, Small I (2006) Recent surprises in protein targeting to mitochondria and plastids. Curr Opin Plant Biol **9:** 610–615

Moffatt BA, Ashihara H (2002) Purine and pyrimidine nucleotide synthesis and metabolism. *In* CR Somerville, EM Meyerowitz, eds, The Arabidopsis Book. American Society of Plant Biologists, Rockville, MD, doi: 10.1199/tab.0018, www.aspb.org/publications/arabidopsis/

Murakami S, Strotmann H (1978) Adenylate kinase bound to the envelope membranes of spinach chloroplasts. Arch Biochem Biophys **185:** 30–38

Neuhard J, Nygaard P (1987) Purines and pyrimidines. *In* FC Neidhardt, JL Ingraham, BK Low, B Magasanik, M Schaechter, HE Umbarger, eds, *Escherichia coli* and *Salmonella typhimurium*: Cellular and Molecular Biology. American Society for Microbiology, Washington, DC, pp 445–473

Neuhaus HE, Emes MJ (2000) Nonphotosynthetic metabolism in plastids. Annu Rev Plant Physiol Plant Mol Biol **51:** 111–140

Peltier JB, Cai Y, Sun Q, Zabrouskov V, Giacomelli L, Rudella A, Ytterberg AJ, Rutschow H, van Wijk KJ (2006) The oligomeric stromal proteome of Arabidopsis thaliana chloroplasts. Mol Cell Proteomics **5:** 114–133

Peltier JB, Ytterberg AJ, Sun Q, van Wijk KJ (2004) New functions of the thylakoid membrane proteome of Arabidopsis thaliana revealed by a simple, fast, and versatile fractionation strategy. J Biol Chem **279:** 49367–49383

Pradet A, Raymond P (1983) Adenine-nucleotide ratios and adenylate energy-charge in energy-metabolism. Annu Rev Plant Physiol Plant Mol Biol **34:** 199–224

Regierer B, Fernie AR, Springer F, Perez-Melis A, Leisse A, Koehl K, Willmitzer L, Geigenberger P, Kossmann J (2002) Starch content and yield increase as a result of altering adenylate pools in transgenic plants. Nat Biotechnol **20:** 1256–1260

Reinhold T, Alawady A, Grimm B, Beran KC, Jahns P, Conrath U, Bauer J, Reiser J, Melzer M, Jeblick W, et al (2007) Limitation of nocturnal import of ATP into Arabidopsis chloroplasts leads to photooxidative damage. Plant J **50:** 293–304

Reiser J, Linka N, Lemke L, Jeblick W, Neuhaus HE (2004) Molecular physiological analysis of the two plastidic ATP/ADP transporters from Arabidopsis. Plant Physiol **136:** 3524–3536

Rosso MG, Li Y, Strizhov N, Reiss B, Dekker K, Weisshaar B (2003) An Arabidopsis thaliana T-DNA mutagenized population (GABI-Kat) for flanking sequence tag-based reverse genetics. Plant Mol Biol **53:** 247–259

Rudolph MG, Veit TJH, Reinstein J (1999) The novel fluorescent CDP-analogue (Pbeta)MABA-CDP is a specitic probe for the NMP binding site of UMP/CMP kinase. Protein Sci **8:** 2697–2704

Schlattner U, Wagner E, Greppin H, Bonzon M (1996) Chloroplast adenylate kinase from tobacco: purification and partial characterization. Phytochemistry **42:** 589–594

Schmid M, Davison TS, Henz SR, Pape UJ, Demar M, Vingron M, Schölkopf B, Weigel D, Lohmann JU (2005) A gene expression map of *Arabidopsis thaliana* development. Nat Genet **37:** 501–506

Schröder M, Giermann N, Zrenner R (2005) Functional analysis of the pyrimidine de novo synthesis pathway in solanaceous species. Plant Physiol **138:** 1926–1938

Schünemann D, Borchert S, Flugge UI, Heldt HW (1993) ADP/ATP translocator from pea root plastids (comparison with translocators from spinach chloroplasts and pea leaf mitochondria). Plant Physiol **103:** 131–137

Schwender J, Ohlrogge J, Shachar-Hill Y (2004) Understanding flux in plant metabolic networks. Curr Opin Plant Biol **7:** 309–317

Small I, Peeters N, Legeai F, Lurin C (2004) Predotar: a tool for rapidly screening proteomes for N-terminal targeting sequences. Proteomics **4:** 1581–1590

Spencer MWB, Casson SA, Lindsey K (2007) Transcriptional profiling of the Arabidopsis embryo. Plant Physiol **143:** 924–940

Spurr AR (1969) A low-viscosity epoxy resin embedding medium for electron microscopy. J Ultrastruct Res **210:** 57–69

Stasolla C, Katahira R, Thorpe TA, Ashihara H (2003) Purine and pyrimidine metabolism in higher plants. J Plant Physiol **160:** 1271–1295

Steinhauser D, Usadel B, Luedemann A, Thimm O, Kopka J (2004) CSBDB: a comprehensive systems-biology database. Bioinformatics **20:** 3647–3651

Stitt M, Lilley RM, Gerhardt R, Heldt HW (1989) Metabolite levels in specific cells and subcellular compartments of plant leaves. Methods Enzymol **174:** 518–550

Stitt M, Lilley RM, Heldt HW (1982) Adenine nucleotide levels in the cytosol, chloroplasts and mitochondria of wheat leaf protoplasts. Plant Physiol **70:** 971–977

Thimm O, Bläsing O, Gibon Y, Nagel A, Meyer S, Krüger P, Selbig J, Müller LA, Rhee SY, Stitt M (2004) MAPMAN: a user-driven tool to display genomics data sets onto diagrams of metabolic pathways and other biological processes. Plant J **37:** 914–939

Usadel B, Nagel A, Steinhauser D, Gibon Y, Blasing OE, Redestig H, Sreenivasulu N, Krall L, Hannah MA, Poree F, et al (2006) PageMan: an interactive ontology tool to generate, display, and annotate overview graphs for profiling experiments. BMC Bioinformatics **7:** 535

Usadel B, Nagel A, Thimm O, Redestig H, Blaesing OE, Palacios-Rojas N, Selbig J, Hannemann J, Piques MC, Steinhauser D, et al (2005) Extension of the visualisation tool MapMan to allow statistical analysis of arrays, display of coresponding genes and comparison with known responses. Plant Physiol **138:** 1195–1204

van der Graaff E, Hooykaas P, Lein W, Lerchl J, Kunze G, Sonnewald U, Boldt R (2004) Molecular analysis of the de novo purine biosynthesis in solanaceous species and in *Arabidopsis thaliana*. Front Biosci **9:** 1803–1816

Wagner KG, Backer AI (1992) Dynamics of nucleotides in plants studied on a cellular basis. Int Rev Cytol **134:** 1–84

Wittwer CT, Ririe KM, Andrew RV, David DA, Gundry RA, Balis UJ (1997) The LightCycler: a microvolume multisample fluorimeter with rapid temperature control. Biotechniques **22:** 176–181

Yoo S-D, Cho Y-H, Sheen J (2007) *Arabidopsis* mesophyll protoplasts: a versatile cell system for transient gene expression analysis. Nat Protoc **2:** 1565–1572

Zhou L, Lacroute F, Thornburg R (1998) Cloning, expression in *Escherichia coli*, and characterization of *Arabidopsis thaliana* UMP/CMP kinase. Plant Physiol **117:** 245–254

Zrenner R, Stitt M, Sonnewald U, Boldt R (2006) Pyrimidine and purine biosynthesis and degradation in plants. Annu Rev Plant Biol **57:** 805–836